# FLORE
# Repository istituzionale dell'Università degli Studi di Firenze

## Computational Speciation Models: A Tool for the Interpretation of Spectroelectrochemistry for Catalytic Layers under Operative

# Computational Speciation Models: A Tool for the Interpretation of Spectroelectrochemistry for Catalytic Layers under Operative Conditions

G. Montegrossi,[a] A. Giaccherini,[b,z] E. Berretti,[b] F. Di Benedetto,[a,c] M. Innocenti,[b,*,z] F. d'Acapito,[d] and A. Lavacchi[e]

[a]IGG, CNR, Florence 50121, Italy
[b]Department of Chemistry, Università degli Studi di Firenze, Florence 50019, Italy
[c]Department of Earth Sciences, Università degli Studi di Firenze, Florence 50019, Italy
[d]IOM, CNR, c/o ESRF, Grenoble 38043, France
[e]ICCOM,CNR, Florence 50019, Italy

In this study, the first coupled FEXRAV and chemical speciation modelling study of the Pd deactivation is presented. Due to the high brilliance of synchrotron light, FEXRAV can investigate deeply buried surfaces. More specifically, we directly analyzed the evolution of the Pd/C catalytic layer during a voltammetric cycle, through a specifically designed electrochemical cell. Still, we observed a complex interfacial chemistry of Pd, which impairs a straightforward interpretation of FEXRAV data. Exploiting thermodynamic chemical speciation modelling we were able to overcome this issue. The study leads to three main results: 1) the confirmation of the relationship between the change of the Pd/Pd(II) ratio and the change of the Fluorescence intensity 2) the investigation of the deactivation mechanism 3) the identification of the relevant species leading to the electrodissolution of Pd under operative conditions. This study opens new perspectives for the application of the chemical speciation modelling to the study of the deactivation mechanism of Pd in Pd/C catalytic layers under operative conditions in different electrolytes.

In recent times, Palladium-based electrocatalysts proved to be able to promisingly substitute Pt in several electrocatalytic applications due to their lower cost and higher availability.[1] Moreover, Pd catalysts resulted very effective in direct alcohol fuel cell (DAFC). One of the benefits consists in the bypass of the deactivation process occurring in Pt catalysts due to reaction with CO.[2,3] Nowadays, the main issue still preventing full exploitation of such electrodic materials is their anodic deactivation, which is not fully understood and manageable. In fact, although the origin of the deactivation has been related to the formation of an oxide layer on the Pd surface, its formation mechanism is still an open question.[4] Moreover, other studies suggested that Pd electrodes are also subjected to electrodissolution under operative condition.[5] In principle, the latter process is competitive with the formation of the oxide layer and it is not observable by means of ex-situ techniques. In this context, a natural follow-up of the conventional ex-situ experiments are in situ/operando spectroelectrochemical measurements, performed to investigate the competition between these two processes under operative conditions. For operative conditions, we refer to the strongly anodic and basic conditions usually applied to the catalytic layer for the electrooxidation of alcohols. In the same context, the catalytic layer is usually intended as the place where the interaction between the electrolyte, the catalysts and the support occurs.[6] Several in-situ/operando techniques applied to catalysts are reported in literature, most of them are carried out on model systems with specific surface preparation or they require concentrated materials (i.e. on Pd electrodes).[7–10] As shown by Minguzzi et al., the Fixed Energy X-ray Absorption Voltammetry[11] enables the direct study of the oxidation state for chemical species under operando conditions. Recently, our group reported an operando study of Pd half-cell through FEXRAV.[12] Our results pointed out that FEXRAV alone is not able to clearly distinguish the different species of the same valence state (i.e. Pd(II)). Hence, even considering only the contribution due to the formation of the oxide layer (PdO) and the electrodissolution of Pd (Pd$^{2+}$ solvated species) to the deactivation process of Pd/C electrocatalyst, the analysis of the experimental data could not identify which

process is prevailing. On this basis, our aim is to present an integrated theoretical-experimental method to draw a conclusion on this subject.

## Methods

***Details of the FEXRAV experiment.***—Recording the time evolution of the sample response to X-rays at a fixed energy close to the absorption edge of an element, FEXRAV reckons the valence states of such element even in a complex matrix under an electrochemical stimulus (i.e. during a cyclic voltammetry).[11,13] Thanks to the high penetration of X-rays, it delivers information on X-ray absorption data through the walls of an electrochemical cells, with only minor design changes with respect to a standard electrochemical cell. Thus, it constitutes an ideal tool to investigate standard catalytic layers in operative conditions. In the setup hereby discussed, the lower detection limit is evaluated to be approximately $10^{13}$ atoms/cm$^2$. In order to perform our experiments we used a standard three electrode cell, specifically designed (3D model in Figure 1a) to be mounted in the experimental XAS chamber of the LISA beamline at ESRF.[14] The schematic of the experimental setup is presented in Figure 1b.

In the FEXRAV study of the Pd half cell, Pd/C nanostructured catalysts were involved. The Pd/C catalysts were synthesized according to the procedure reported in Refs. 15,16. The anode catalytic ink was prepared by mixing and sonicating the Pd/C catalyst (100 mg) with water (400 mg) and a 5 wt% nafion solution. The final charge of Pd on the electrode is approximately 4 mg/cm$^2$, a target loading selected to achieve the optimal sensitivity in the FEXRAV experiment. The electrochemical measurements have been performed by means of a PAR263 potentiostat installed at the BM08 beamline. The results obtained studying two different electrolytic solutions are presented in this paper: 1) KOH 2 M and 2) EtOH 2 M + KOH 2 M.

Concerning the beamline set up, the monochromator was equipped with Si(311) flat crystals, with an energy resolution $\Delta E/E \approx 10^{-5}$, a spot size of about 2*0.5 mm and a flux at the sample position up to
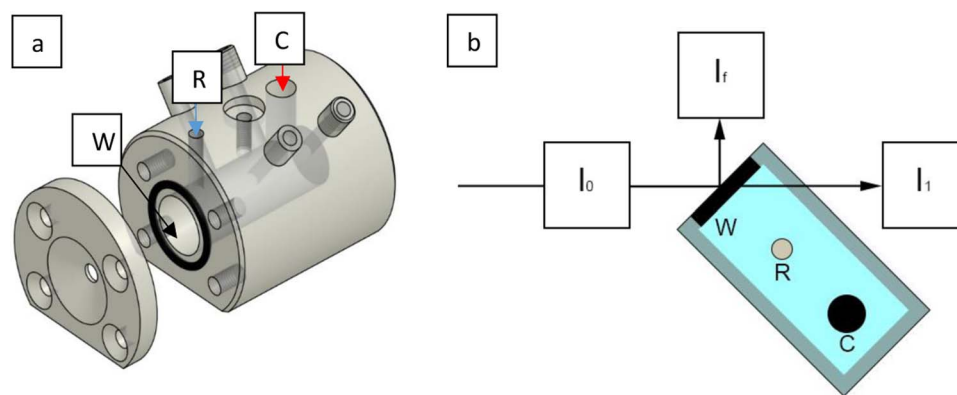
**Figure 1.** a) 3D model of the electrochemical cell used during the FEXRAV measurements with the position of the working electrode (W), reference electrode (R) and counter electrode (C); b) experimental setup for fluorescence (If) and transmission (I1) measurements. I0 is the incoming monochromatic X-ray radiation.

$10^{10}$ ph/s. All spectra were registered at room temperature, with reference to a metal foil, simultaneously analyzed in a second chamber located after the former. According to this procedure, the energy calibration was let available during the whole measurement. Reference materials were: elemental Pd under the form of a metal foil (Goodfellow) and PdO (Sigma Aldritch). This latter sample was prepared dispersing and homogenizing an appropriate amount of microcrystalline powders in cellulose, and pressing the mixture to a self-supporting half inch pellet.

*Numerical modelling.—Phreeqc formalism.*—We performed our calculation under the *phreeqc* formalism,[17] taking into account aqueous species equilibria in a reference database. The solid phases are considered through dissolution/precipitation reactions, and their stability is reported as the logarithm of equilibrium constant of formation (log K) at standard temperature and pressure condition (i.e. 25°C and 1.0132 bar) from the master species.[18,19] Only one master species is associated to each element or element valence state (for instance $Fe^{3+}$ for ferric iron), one to the hydrogen ion, one to water and (formally) one to the aqueous electron. In this work, $Pd^{2+}_{(aq)}$ acts as master species while all the other species coming from the dissolution of metallic Pd in the half cell are secondary species ($Pd(OH)^{+}_{(aq)}$, $Pd(OH)_2$, $Pd^{+}_{(aq)}$, etc.). The master species are the "building blocks" used in the *phreeqc* formalism to write all chemical equations: they are related to the secondary species, in fact, by means of formation reactions involving the master species as a reactant (e.g. $Pd^{2+} + 2OH^{-} = Pd(OH)_2$, $Pd^{2+} + e^{-} = Pd^{+}$, etc.) and the relative equilibrium constant logarithms are included in the calculation (as a function of temperature). These species are present in a single phase, an aqueous solution. On this ground, the aim of the *phreeqc* formalism is the definition of a system of algebraic homogeneous equations describing the equilibrium conditions for different thermodynamics variables such as the activities of aqueous species (including water), ion-exchange species, surface-complexation species, gas-phase components, solid solutions, pure phases, aqueous charge balance, gas-phase equilibria and ionic strength. Such algebraic system is assembled taking into considerations all the residual function (denoted by *f*) describing the relevant equilibria. The residual functions are defined as the difference between a global constant and the combination of specific variables for each species or phases. Hence, for each set of values of the thermodynamics variables, defining a certain state of the system, the residual functions describe the "distance" of the state from the equilibrium. On this basis, the equilibrium condition corresponds to the set of values for the thermodynamics variables that let all the residual functions equal to zero. To compute the results, each residual function is reduced to contain a minimum number of variables (called the unknown masters), so that the number of functions equals the number of variables. The unknown masters for aqueous solutions are the natural log of the activities of master species ($\ln a_m$), the natural log of the

activity of water ($\ln a_{H_2O}$), the ionic strength ($\mu$), and the mass of solvent water in an aqueous solution ($W_{aq}$). The system is then computed and solved by means of the Newton-Raphson technique, which proceeds through the assembling of a Jacobian matrix containing the derivatives of the residual functions by the unknown master. Thus, this matrix describes the thermodynamics of the multi-equilibria system and its diagonalization leads to the equilibrium conditions. The analytic expression of each residual function and of the related derivatives has been developed and implemented in the *phreeqc* software. For instance, the equilibrium between the aqueous phase and pure solid phases is described under the following assumptions:

1) The activity of the pure phase is 1.0
2) The additional unknown master for each pure solid phase is the mole of the pure phase present in the system ($n_p$ where p refers to the $p^{th}$ phase)
3) The mass-action law holds

Under this assumptions the pure phase equilibria are described by the mass-action law:

$$K_p = \prod_m^{M_{aq}} a_m^{C_{m,p}}$$

Where $K_p$ is the equilibrium constant with the $p^{th}$ phase, $c_{m,p}$ is the stoichiometric coefficient of the aqueous master species (positive if the product of the desorption reaction and negative otherwise), $a_m$ is the activity of the $m^{th}$ species (it is an unknown master). Eventually, $M_{aq}$ is the number of aqueous master species.

On this basis a new residual function can be defined:

$$f_p = \ln K_p - \sum_m^{M_{aq}} C_{m,p} \ln a_m$$

The total derivative of the residual function in terms of the unknown master is:

$$d f_p = \sum_m^{M_{aq}} c_{m,p} \, d \ln a_m$$

Chemical speciation in aqueous solutions is not uniquely defined but depends on the theoretical formulation of mass-action equilibria and activity coefficients (e.g. Davis, Pitzer or Debye-Huckel activity model);[17] in other words, the numerical solution of the system is model-dependent. Some aqueous speciations can be analytically determined, but operational definitions and assumptions are still unavoidable. Accordingly, the equilibrium is computed with a reaction-path calculation, i.e. a sequence of mass-transfer calculations that follows defined phase (or reaction) boundaries during incremental steps of reaction progress.
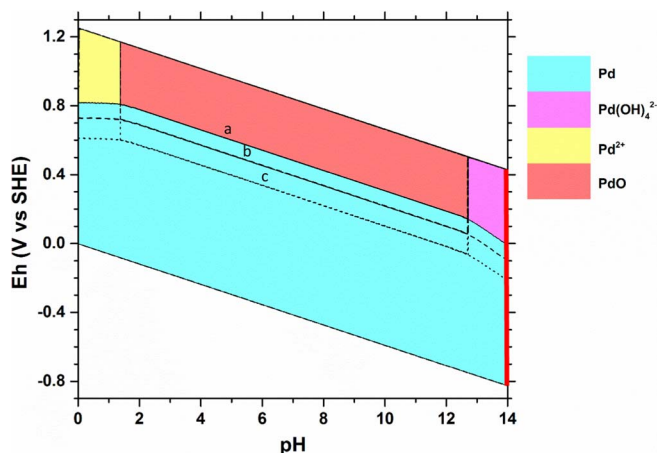
**Figure 2.** Pourbaix diagrams of the Pd-O-H system a) [Pd] = $1 \cdot 10^{-3}$ mol/kgw b) [Pd] = $1 \cdot 10^{-6}$ mol/kgw c) [Pd] = $1 \cdot 10^{-10}$ mol/kgw.

In this study, the considered gas species, i.e. $H_{2(g)}$ and $O_{2(g)}$, are computed defining the corresponding partial pressures, and in the database are present the dissolution reactions (e.g. $O_{2(g)} = O_{2(aq)}$) and the corresponding constants. Accordingly, the presence of oxygen or hydrogen in any redox reaction is linked to their partial pressures. These latter are monitored as the result of an evolving chemical system in any given thermodynamic conditions.

*The Pd-O-H system.*—Numerical models for the chemical speciation require comprehensive thermodynamic databases. Although today's geochemical databases are quite complete, including the most common reactions and reaction constants, some equilibria typical of specific environments may be not present. Accordingly, the thermodynamic properties of some chemical species relevant to our model have been checked, and added, to the *phreeqc* wateq4f.dat database.[20] Specifically, Palladium hydroxylates have been added according to the work of Mountain and Wood.[21]

*Modelling of the predominance charts and of the FEXRAV signals.*—In the present study, the relationships between the main phases of the Pd-O-H system (Pd and water solution) are studied through the use of Eh versus pH (or "*Pourbaix*") diagrams, calculated according to the point-by-point mass balance method (referred also as the grid method).[22,23] Under this approach, a grid is defined by the span of the potential (Eh – with respect to the standard hydrogen electrode), pH and the chosen resolution (0.01 logarithmic units in both the Eh and pH axes, in the present case). Then, the chemical speciation for a given total amount of the element of interests is computed according to the *phreeqc* formalism[22] for each given point of the grid. The results are rendered directly by coloring each species differently and plotting each point of the grid with the color of the predominant species (as depicted in Figure 2). The predominant species (in the aqueous or solid phase) is identified as the species with the highest amount (moles) at the equilibrium.

The modelling of the FEXRAV signal relies on its dependence on the Pd chemical speciation in the Pd-O-H system. For a given amount of Pd, the chemical speciation is computed at each potential applied during the voltammetric scan. Thus, the Pd-bearing species exhibiting the higher amount of moles is considered prevalent, whereas species with an amount less than $10^8$ times lower than the former are neglected in the presentation of the results.

## Results

*Pourbaix predominance charts.*—The predominance charts were computed in a grid limited by the conventional water stability field from 0 to 14 pH units. The choice of the concentration of the master

species were dictated by the possibility of an immediate comparison with selected Pourbaix diagrams available in the literature: Mountain and Wood,[21] Naoto[24] and Pourbaix et al.[25] It is noteworthy to mention that the former articles refer to calculations performed using the mass balance method, and including results calculated by using up to five different databases, whereas the latter presents results obtained using the "line method" (i.e. depicting the boundary defined by Nernst equations). Figure 2 shows the Pourbaix diagram for the Pd-O-H system, where our point-by-point mass balance approach leads to very close agreement with all the cited works. Only a small difference can be evidenced between the Pourbaix et al.[25] study and the present one, and near the stability boundary of water, where our calculations predict the predominance of $Pd(OH)_4^{2-}$ (Palladium tetrahydroxilate), whereas Pourbaix et al. reports $PdO_2^{2-}$.[25]

As the total amount of Pd assumed in the calculation increases, the only changes in the plot deal with the Pd/Pd(II) boundary, because higher Pd contents stabilize the solid phases. This is due to fact that Pd solubility, dependent on speciation, is in any case limited. Under the operative conditions (pH = 14 and anodic potential), the relevant boundary is $Pd/Pd(OH)_4^{2-}$ while the fractional amount of PdO is generally two orders of magnitude lower with respect to both Pd and $Pd(OH)_4^{2-}$.

*Fluorescence.*—The simultaneous acquisition of the electrochemical and FEXRAV signals from the electrodic layer required a specific choice of the energy of the incident X-ray beam. Figure 3a depicts two X-ray Absorption Near Edge Spectroscopy (XANES) spectra of the reference materials, Pd and PdO. The difference between the XANES spectra of Pd and PdO is apparently maximized at 24370 eV. It is worth to notice that at this energy, the higher is the signal intensity, the lower is the fraction of Pd(0) contributing to the signal. On this ground, FEXRAV signals have been registered by means of the Fluorescence detector, while performing a cyclic voltammetry from −0.2 V to 1.2 V (RHE) with a scan rate of 1 mV/s, irradiating the electrochemical cell with a monochromatic persistent beam set up at 24370 eV. Apparently, at anodic potential we observe an increased signal intensity, and at the end of the cathodic scan the fluorescence signal is lower than at the beginning of the anodic scan (Figure 3b).

*Speciation.*—The chemical speciation modelling of this system under the voltammetric stress can be efficiently implemented defining analytical fractional amount readily usable. To this end, we calculated a 'slice' of the Pourbaix diagram in operative condition (red vertical line in Figure 2) corresponding to the range of potential applied to the electrode. Then a polynomial function has been fitted on the numerically calculated fractional amounts against Eh. Such function constitute the esteem of the fractional amount, as a function of Eh, used to follow the chemical speciation during the voltammetry. The speciation models revealed that Pd and $Pd(OH)_4^{2-}$ are the most relevant species. In fact, the third species by abundance (PdO) has a fractional amount not higher than $3 \cdot 10^{-4}$ while the other Pd-bearing species are always lower than $10^{-7}$. Regarding the effect of ethanol on the equilibrium speciation the results for a KOH 2 M and EtOH 2 M solution are equivalent to the one for the solution KOH 2 M since the only effect of the EtOH at the equilibrium is to be oxidized to $CO_2$ and $H_2O$. However the reaction is so slow that it has no practical meaning in our context. Hence, for our purposes the Pd-O-H and Pd-C-O-H systems are equivalent.

*Comparison between experiment and modelling.*—Figure 4 shows the FEXRAV data for a KOH 2 M solution together with the corresponding calculated speciation distribution. The FEXRAV signal shows a periodic oscillation in response to the potential ramps. A further apparent feature of Figure 4, is that the oscillation between maxima and minima in the FEXRAV signal (whose shape, amplitude and phase are almost constant throughout the whole experiment) are combined with a general linear trend decreasing the signal intensity. This suggest that FEXRAV intensity is eventually not only determined by alternation of different redox states of solid Pd-bearing species.
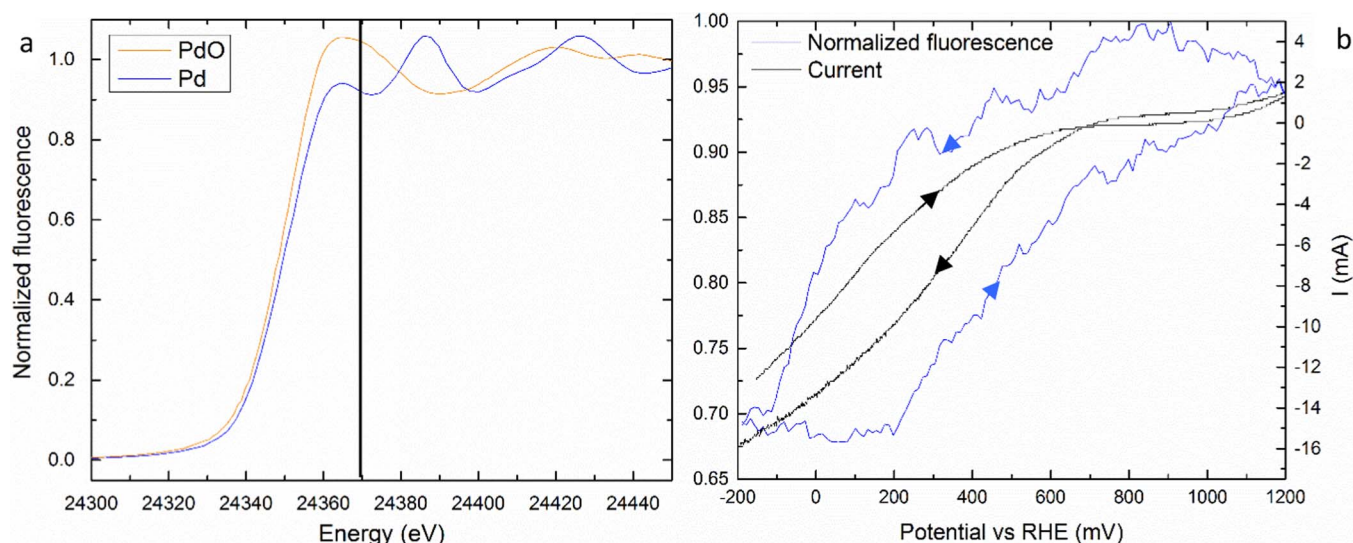
**Figure 3.** a) XANES spectrum for Pd and PdO standards b) The black curve is the current measured and the blue curve is the fluorescence signal from the electrode interface in a KOH 2 M solution.

The speciation model is in close agreement with the FEXRAV signal. Since the fractional amounts result from the equilibrium computation, their maxima and minima correspond, as expected, to the maxima and minima of the potential ramps. One can notice that the maxima of the FEXRAV occur after (approximately 0–200s) the maxima of the fractional amount of $Pd(OH)_4^{2-}$ in the catalytic layer. In the same way, the minima of the FEXRAV occur after (approximately 1000–1400s) the maxima of the fractional amount for Pd. This pattern is constantly reproduced for all the performed voltammetric cycles.

Figure 5 depicts the comparison between the results of a FEXRAV experiment (KOH 2 M and EtOH 2 M) solution with the speciation calculations for a KOH 2 M. Again, a good agreement between experimental data and the speciation model is achieved for all the voltammetric cycles. If compared to Figure 4, the main difference is the shape of the oscillations. For the solution of KOH and ethanol, the oscillation amplitude appears wider than with a solution of KOH only. Regarding the general trend of decreasing intensity observed in the FEXRAV of the half-cell filled with KOH, an almost linear decrease is observed also in the case of KOH and ethanol, but it is limited up to the 4th voltammetric cycle, whereas after the 5th cycle a pseudo steady state is established. Interestingly, the ethanol in the electrolyte seems to make the maxima (or minima) of the FEXRAV signal occurring before the maxima (or minima) of the fractional amount for $Pd(OH)_4^{2-}$ along all the voltammetric cycles. This trend is clearly opposite to what observed in Figure 4.

## Discussion

The Pourbaix diagrams of Figure 2, used to model the chemical speciation of the Pd-O-H, reveal an excellent agreement with the literature. No differences between the present and the latest published stability fields[21,24] are observed. The only small difference was found in the comparison with the Pourbaix et al. findings,[25] who couldn't take in account the chemistry of hydroxypalladiates at the time. In their paper, these authors reported the diagrams with the hypothetical predominance of $PdO_2^{2-}$ ions where we find the predominance of $Pd(OH)_4^{2-}$. As discussed by Pourbaix et al. themselves, the confirmation of their hypothesis was impaired by the lack of a thorough thermochemical characterization of hydroxypalladiates. However, the predominance of $Pd(OH)_4^{2-}$ was firstly predicted by Mountain and Wood[21] exploiting the thermochemical characterization published by Chandrasekharam in 1974.[26] The latter was not accounted before 1988 when Mountain and Wood[21] applied the mass balance method to de-

scribe hydrothermal processes involving Pd species. An almost perfect agreement occurs between the present and Mountain and Wood's[21] charts. It is our opinion that the reproducibility of the literature's predominance charts by our approach enables its use as a tool to predict the evolution of chemical speciation in the Pd-O-H system during a voltammetric scan. Following the Mountain and Wood's calculation, the role played by the $Pd(OH)_4^{2-}$ species appears crucial for the interpretation of FEXRAV data.

Regarding the comparison between simulated and experimental FEXRAV data, the first part of this discussion is focused on the analysis of the chosen electrochemical and spectroscopic operating conditions. These conditions were, in fact, dictated by a mediation between the requirements of both voltammetry and XAS spectroscopy. At least two main choices are relevant:

1)  The choice of monitoring FEXRAV through the Fluorescence detector is due to the sampling depth of the relative signal. At 24370 eV, the attenuation length of X-rays in the catalytic layer is estimated around 10 μm (i.e. smaller than the layer thickness).[6,27] Hence, the signal received by the Fluorescence detector is relative only to the catalytic layer.

2)  The very low scan rate (1 mV/s) was aimed at improving the sampling time and to achieve the best possible signal-to-noise ratio (SNR) in the Fluorescence detector. As a side consequence, at this rate the system approaches the Nernstian equilibrium. Thus, the results of our thermochemical description based on the mass balance method (i.e. at the thermodynamic equilibrium) can provide an appropriate description of the chemical environment at the electrodic interface. This reflects the excellent agreement we found between the FEXRAV measurements and the calculated chemical speciation of Pd.

According to the recent literature, the spectral feature at 24370 eV, although being chosen in the present study from the comparison of Pd and PdO XANES spectra, is not specifically diagnostic for PdO, and can be safely used to assess only the generic oxidation of Pd to Pd(II).[28–31] In fact, the XANES signals are mostly sensitive to the oxidation state of an element, and less sensitive to its local coordination and structure.[32] Hence, from the spectroscopic point of view, PdO and $Pd(OH)_4^{2-}$ cannot be easily discriminated, whereas the redox change from Pd to Pd(II) can be easily monitored, even using a single fixed energy of 24370 eV (Fig. 3a).

The comparison between the trend of the current and FEXRAV as a function of the potential in the Figure 3b qualitatively suggests that Pd undergoes the same oxidation process reported in References 28–31
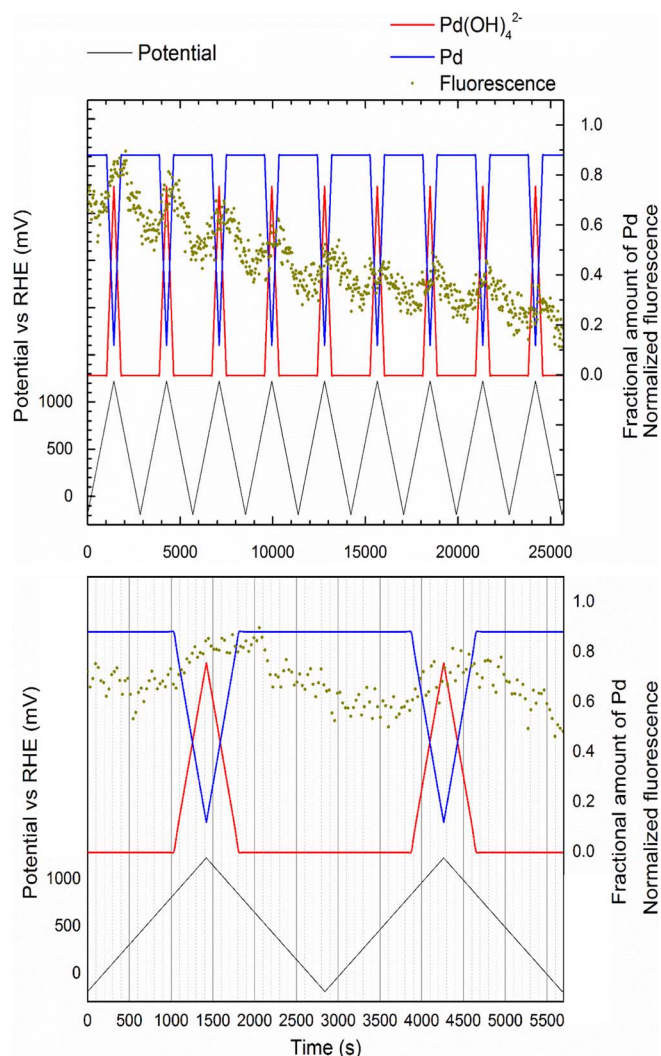
**Figure 4.** Experimental FEXRAV signal and calculated fractional amount of the relevant species, Pd and Pd(OH)$_4^{2-}$, during a potential scan rate of 1 mV/s. The electrochemical cell was mounted in the three electrode scheme, and filled with a KOH 2 M solution. FEXRAV signal was detected through the Fluorescence detector. (a) is the overwiew of the entire voltammetric scan (b) is a closeup of the first two cycles.
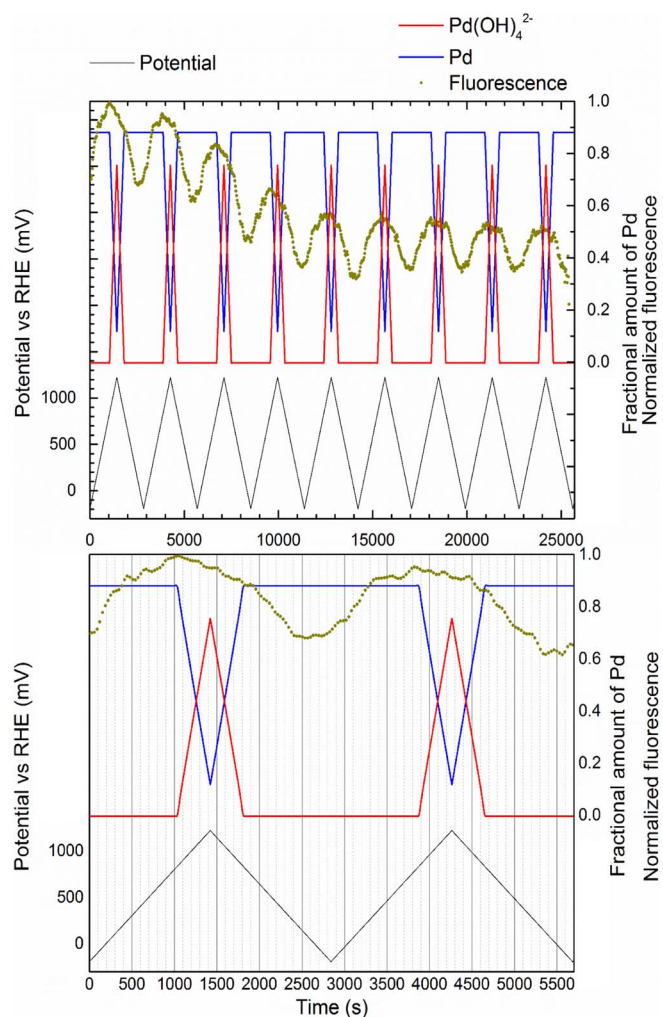


**Figure 5.** Experimental FEXRAV signal and calculated fractional amount of the relevant species, Pd and Pd(OH)$_4^{2-}$, during a potential scan rate of 1 mV/s. The electrochemical cell was mounted in the three electrode scheme, and filled with a KOH 2 M and EtOH 2 M solution. FEXRAV signal was detected through the Fluorescence detector. (a) is the overwiew of the entire voltammetric scan (b) is a closeup of the first two cycles.

However, these works are related to catalytic processes completely different with respect to the oxidation process, observed in the anodic half-cell of a DAFC. Hence, although we expect the oxidation of Pd to Pd(II), we cannot safely confirm that the increase of the FEXRAV intensity in Figure 3b is linked to this phenomenon without a speciation model. The calculated speciation as a function of time (Fig. 4) allowed to conclusively state that the relevant species are Pd and Pd(OH)$_4^{2-}$ and that the fractional amount of PdO is negligible. Indeed, the oscillatory increase of FEXRAV, when applied potential values approach 1000 mV vs RHE, is explained in terms of a temporary predominance of the oxidized Pd(OH)$_4^{2-}$ species over the reduced Pd species.

The explanation of the general decreasing trend, observed in the full experiment with KOH (Fig. 4) and only partially in the experiment with KOH and EtOH (Fig. 5) deserves a further discussion. Since the Pd(OH)$_4^{2-}$ is soluble, the total amount of Pd in the catalytic layer progressively decreases due to the diffusion process. To approximately quantify the effect of the diffusion, we should consider that roughly a quarter of the total time of the voltammetric scan (t $\approx$ 700 s) is spent under diffusion limited condition. In addition, the diffusion coefficient for Pd(OH)$_4^{2-}$ is assumed to be D = 6.14 10$^{-8}$ m$^2$/s.[33,34] On this basis, the thickness of the diffusion layer is 13 mm ($\delta = \sqrt{4Dt}$ [35]).

Thus, both the thickness of the catalytic layer (roughly 100 µm) and the sampling depth for Fluorescence (roughly 10 µm) signal are negligible if compared to the thickness of the diffusion layer. Therefore, the increasing of the diffusion layer thickness over time, depletes the total Pd content from the catalytic layer (hence also the sampling volume), resulting in a net and progressive decrease of the average FEXRAV signal revealed by the Fluorescence detector. These results are in line with the considerations provided by the review study of Grden.[5] Two main differences between the experimental data for the KOH 2 M solution (Figure 4) and the KOH 2 M + EtOH 2 M solution (Figure 5) where revealed:

1)  the fluorescence peaks for the KOH 2 M occur after the correspondent peaks in the speciation model (after the inversion of the potential), whereas the peaks KOH 2 M + EtOH 2 M solution occur before the calculated peaks (before the inversion of the potential);
2)  the decrease of the averaged fluorescence signal is linear for KOH 2 M solution while it stops after the 4$^{th}$ cycle for the KOH 2 M + EtOH 2 M solution.

These discrepancies are probably related to mechanistic and kinetics differences between the process occurring in the two electrolytes, and deserve further investigations, still in progress.

## Conclusions

In this paper we present a modelling procedure of the chemical speciation (namely the mass balance method) which proved to be very useful in the interpretation of the results recorded by means of a new application of the FEXRAV technique.

Basically, we have shown that while experimental FEXRAV data registered through the Fluorescence detector can easily correlate with the potential applied to a Pd-bearing catalytic layer, an attribution of the changes in the chemistry responsible of the the changes in the FEXRAV signal cannot be appropriately reached. The proposed numerical modelling approach clearly points out a chemical speciation dependent on the applied potential where changes of the relative amounts of Pd and Pd(II) are responsible for the change of FEXRAV intensity during the voltammetric scan. Moreover, we were able to identify the main Pd(II) species involved in the process was identified as $Pd(OH)_4^{2-}$. On this ground, our study was able to confirm the prevalence, under the operative conditions, of the electrodissolution processes of Pd over the formation of the oxide layer.

It is opinion of the authors that this approach is of general interest in helping the analysis of data coming from spectroscopic techniques used to detect speciation features, in particular when working near equilibrium.

## References

1. European Commission, *Critical Raw Materials for the EU*, (2010).
2. V. Bambagioni et al., *ChemSusChem*, **5**, 1266 (2012).
3. C. Bianchini and P. K. Shen, *Chem. Rev.*, **109**(9), 4183 (2009).
4. L. Wang et al., *Electrochim. Acta*, **177**, 100 (2015).
5. M. Grdeń, M. Łukaszewski, G. Jerkiewicz, and A. Czerwiński, *Electrochim. Acta*, **53**, 7583 (2008).
6. A. Lavacchi, H. Miller, and F. Vizza, *Nanotechnology in Electrocatalysis for Energy*, 115, (2013).
7. F. Zaera, *Chem. Soc. Rev.*, **43**, 7624 (2014).
8. B. L. Mojet, S. D. Ebbesen, and L. Lefferts, *Chem. Soc. Rev.*, **39**, 4643 (2010).
9. S. Campisi et al., *J. Phys. Chem. C*, **120**, 14027 (2016).
10. L. Wang et al., *J. Power Sources*, **195**, 8036 (2010).
11. A. Minguzzi et al., *Anal. Chem.*, **85**, 7009 (2013).
12. D. G. Montegrossi, D. A. Giaccherini, D. F. Di Benedetto, D. W. Giurlani, and D. A. Lavacchi, in *MSE*, (2016).
13. E. Achilli et al., *Journal of Spectroscopy*, **2014**(2014).
14. A. Balerna et al., *Not Neutroni Luce Sincrotrone*, **19**, 14 (2014).
15. P. K. Shen and C. Xu, *Electrochem. commun.*, **8**, 184 (2006).
16. C. Xu, P. kang Shen, and Y. Liu, *J. Power Sources*, **164**, 527 (2007).
17. B. D. L. Parkhurst and C. a J. Appelo, *Exch. Organ. Behav. Teach. J.*, **D**, 326 (1999).
18. H. C. Helgeson, J. M. Delany, H. W. Nesbitt, and D. K. Bird, *Am J Sci*, **278–A** (1978).
19. J. W. Johnson, E. H. Oelkers, and H. C. Helgeson, *Computers & Geosciences*, **18**(7), 899 (1992).
20. J. W. Ball and D. K. Nordstrom, *U.S. Geol. Surv. Water-Resources Investig. Rep.*, **91–183**, 1 (1991).
21. B. Mountain and S. A. Wood, *Economic Geology*, **83**(3), 492 (1988).
22. H. Huang, *Metals*, **6** (3), 23 (2016).
23. A. Giaccherini, G. Montegrossi, and F. Di Benedetto, *Minerals*, **6**, 79 (2016).
24. N. Takeno, *Natl. Inst. Adv. Ind. Sci. Technol. Tokyo*, 285 (2005).
25. M. J. N. Pourbaix, J. Van Muylder, and N. de Zoubov, *Platin. Met. Rev.*, **3**, 47 (1959).
26. M. Chandrasekharan, M. R. Udupa, and G. Aravamudan, *Press. Pergamon Britain, Gt. Discuss. Exp.*, **36**, 1417 (1974).
27. B. L. Henke, E. M. Gullikson, and J. C. Davis, *At. Data Nucl. Data Tables*, **54**, 181 (1993).
28. J. B. Brazier et al., *Catal. Struct. React.*, **3**, 54 (2017).
29. D. Koziej et al., *Phys. Chem. Chem. Phys.*, **11**, 8620 (2009).
30. G. L. Chiarello and D. Ferri, *Phys. Chem. Chem. Phys.*, **17**, 10579 (2015).
31. J. Nilsson et al., *ACS Catal*, **5**, 2481 (2015).
32. M. Newville, *Rev. Mineral. Geochemistry*, **78**, 33 (2014).
33. W. P. Griffith, S. D. Robinson, and K. Swars, *Gmelin Handbook of Inorganic Chemistry - Pd*, (1989).
34. R. Visomirskis and Y. L. Morgenstern, *Liet. TSR Moksl. Akad. Darbai S*, **1**, 49 (1966).
35. A. J. Bard et al., *Electrochemical Methods Fundamentals and Applications*, (2000).